ACS Sustainable Chemistry & Engineering

Research Article

pubs.acs.org/journal/ascecg

Methane Hydrate Formation Promoted by $-SO_3^-$-coated Graphene Oxide Nanosheets

Fei Wang,*[,†,‡,∥] Han-Lin Meng,[§,∥] Gang Guo,[†] Sheng-Jun Luo,*[,†] and Rong-Bo Guo*[,†]

[†]Shandong Industrial Engineering Laboratory of Biogas Production & Utilization, Key Laboratory of Biofuels, Qingdao Institute of Bioenergy and Bioprocess Technology, Chinese Academy of Sciences, Qingdao 266101, Shandong, China

[‡]University of Chinese Academy of Science, Beijing 10049, China

[§]Ocean University of China, Qingdao 266110, China

Supporting Information

ABSTRACT: Sodium dodecyl sulfate (SDS) has been reported as the most efficient kinetic promoter for hydrate-based natural gas storage and transportation; however, the foam generation during hydrate dissociation is a serious problem. In this work, we grafted the $-SO_3^-$ group (similar as the hydrophilic group of SDS) on nanosheets of graphene oxide (GO) to prepare $-SO_3^-$-coated GO nanosheets (sulfonate graphene oxide, SGO), which were then used to promote methane hydrate formation. For comparison, graphene (GP) and GO were also prepared and used as kinetic promoters for methane hydrate formation. Among SGO, GP, and GO, SGO produced the best promotion, which at concentrations of 0.25, 0.5, 0.75 g/L resulted in methane hydrate formation finished within 208.7 ± 26.6, 242.3 ± 97.6, and 312 ± 135.5 min, respectively, with storage capacities reaching 139.7 ± 4.7, 143.3 ± 6.1, and 143.9 ± 7.2 v/v, respectively. Furthermore, $-SO_3^-$-coated nanosheets of SGO even produced better promotion to methane hydrate formation compared with SDS and avoided foam generation during hydrate dissociation, which has great potential in hydrate-based natural gas storage and transportation.

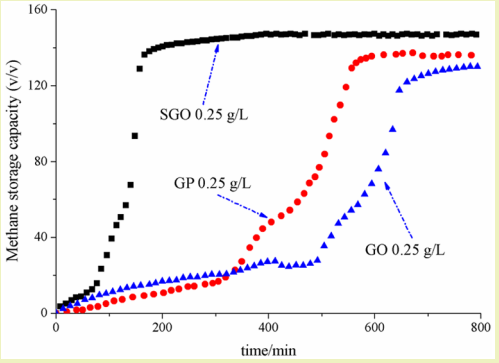

KEYWORDS: *Methane hydrates, Graphene, Graphene oxide, Sulfonated graphene oxide, Promotion*

INTRODUCTION

Gas hydrates, formed by water and gas molecules under suitable pressure and temperature,[1] have been considered with potential for natural gas storage transportation since the 1990s due to high storage capacity and moderate storage condition.[2,3] However, the long induction period and slow growth rate during hydrate formation seriously impacted the application in natural gas storage and transportation.[4] Therefore, it is very necessary to achieve rapid hydrate formation together with high storage capacity for the utilization of gas hydrates.

Many researchers have applied surfactants to promote gas hydrate formation.[4−13] For example, Zhong and Rogers[4] reported that SDS above 242 ppm could accelerate ethane hydrate formation more than 700 times. Lin et al.[5] reported that SDS of 600−1600 ppm resulted in methane hydrate growth finished within 30 min and methane consumption of about 0.008 mol gas/g water (142.7 v/v). Ganji et al.[6] used anionic SDS, cationic cetyltrimethylammonium bromide (CTAB), and nonionic ethoxylated nonylphenol (ENP) to promote methane hydrate formation and found that SDS produced the most efficient promotion, which led to hydrate formation at initial 8.3 MPa and 276.2 K completed within 2−3 h, and the final methane consumption reach 0.12−0.14 mol gas/mol water (119−138 v/v). Wang et al.[7] used SDS, SDSN (sodium dodecyl sulfonate), and SDBS (sodium dodecyl benzenesulfonate) of 1−4 mmol/L as kinetic promoters for methane hydrate formation at initial 6 MPa and 275.15 K and concluded that SDS produced the best promotion, which resulted in an induction period of 93 ± 39−153 ± 76 min, hydrate growth period of 30 min, and methane consumption of about 0.12 mol gas/mol water (119 v/v). So far, dozens of surfactants have been applied to promote gas hydrate formation, among which SDS produced the most efficient promotion and therefore caused the most attention.[14] However, the use of surfactants also led to lots of foam generated during gas hydrate dissociation, which not only impacted the application of gas hydrates but also caused a loss of surfactants.[15,16] Therefore, improving the application performance of surfactants or developing novel kinetic promoters is very essential.

During the past decade, graphene has aroused great attention in various fields due to peculiarities, such as good electrical and thermal conductivities, good mechanical properties, etc.[17] As gas hydrate formation is an exothermal reaction, the presence of graphene can remove the heat released from hydrate formation rapidly and therefore may produce efficient promotion to gas

Received: March 20, 2017
Revised: June 4, 2017
Published: June 7, 2017

DOI: 10.1021/acssuschemeng.7b00846
ACS Sustainable Chem. Eng. 2017, 5, 6597−6604

hydrate formation; however, related studies are merely reported by a few researchers.[17−20] Ghozatloo et al.[18] used Hummers' graphene for the first time to promote natural gas hydrate formation at initial 6.9 MPa and 277.15 K and found that graphene of 1 wt % could reduce the induction period by 61.07% and increase the storage capacity by 12.9% compared with deionized water because of the increase in the initial dissolved gas in nanofluids. Afterward, Hosseini et al.[19] used SDS-stabilized graphene nanofluid (graphene of 1 wt %) to promote natural gas hydrate formation and reported that the graphene nanofluid could reduce induction time by 19.2% and increase storage capacity by 7.6% compared to the SDS/water system. Rezaei et al.[20] used graphene oxide and SDS, respectively, to promote ethylene hydrate formation and also reported that graphene oxide produced more efficient promotion to ethylene hydrate formation, indicating that graphene could serve as the substitution of SDS in promoting natural gas hydrate formation. However, Kim et al.[21] reported that the confinement and strong interaction of water with the hydrophilic surface of graphene oxide reduced the water activity and therefore inhibited the phase behavior of gas hydrates. Therefore, more work is needed to clearly understand the effects of graphene and modified graphene on gas hydrate formation.

In this work, we first prepared GP and GO and applied them in methane hydrate formation to study promotion efficiency. Furthermore, given that SDS has been confirmed as the most efficient kinetic promoter for gas hydrate formation, we grafted $-SO_3^-$ groups (similar as the hydrophilic group of SDS) on GO nanosheets through sulfonation to prepare $-SO_3^-$-coated GO nanosheets (SGO), which were then used to promote methane hydrate formation.

EXPERIMENTAL SECTION

Materials. Expansible graphite (325 mesh) was provided by Nangjing Jicang Nano Technology Co., Ltd. (Nangjing, China). Potassium permanganate (A.R.) was purchased from Laiyang Fine Chemical Factory (Laiyang, China). Sodium nitrate (A.R.), sodium *p*-amino benzenesulfonate (A.R.), sodium hydroxide (A.R.), sulfuric acid (95−98%), and hydrochloric acid (36−38%) were purchase from Sinopharm Chemical Reagent Co., Ltd. (Shanghai, China). Sodium nitrite (A.R.) was provided by Tianjin Dengke Chemical Reagent Co., Ltd. (Tianjin, Tianjin). Sodium borohydride (A.R.) was purchased from Chengdu Kelong chemical reagent factory (Chengdu, China). Hydrogen peroxide (H_2O_2, 30%) was purchased from Tianjin Dingshengjin Chemical Reagent Co., Ltd. (Tianjin, China). Hydrazine hydrate (80%) was provided by Tianjin Basf Chemical Industry (Tianjin, China). Ethyl alcohol (80%) was purchased from Tainjin Fuyu Refine Chemical Factory (Tianjin, China).

Preparation of GO. GO used in this work was prepared through the modified Hummers method.[22] First, 230 mL of H_2SO_4 (98%) was added into a conical flask and cooled to 0−4 °C. Second, 10 g of expansible graphite and 5 g of $NaNO_2$ were, respectively, added into the conical flask under magnetic stirring (300 rpm). Third, after the graphite and $NaNO_2$ were completely dissolved, 30 g of $KMnO_4$ was added in six time intervals, and the conical flask was stirred (300 rpm) under 10−15 °C for 2.5 h. Fourth, the conical flask was kept under 35 °C for 30 min and then at 80−100 °C for 30 min after a certain amount of deionized water was added. Fifth, a certain amount of H_2O_2 (5%) was added, and then the reaction solution was filtered. Sixthly, the filter residue was collected and washed with HCl solution (5%) until no SO_4^{2-} could be detected. Seventh, the filter residue was washed with deionized water and dried at 40 °C, and GO was finally obtained.

Preparation of GP. GP was prepared through the reduction of GO. First, 100 μL of hydrazine hydrate was added into 100 mL of GO solution, which was then stirred under 95 °C for 5 h. Afterward, the solution was filtrated, and the filter residue was collected and washed with methenyl trichloride three times, which was then vacuumly dried, and GP was finally obtained.

Preparation of SGO. The preparation of SGO consisted of four steps in this work. During the first step, GO was prereduced. Fifteen milliliters of $NaBH_4$ solution of 40 g/L was added into 75 mL of GO solution of 1 g/L. Afterward, the pH of the GO solution was adjusted to 9−10 with an Na_2CO_3 solution (5%), which was then stirred under 80 °C for 1 h, and the prereduced GO solution was achieved.

During the second step, the *p*-amino benzenesulfonic acid diazonium salt was prepared. Five milliliters of NaOH solution (2%) and 0.5 g of *p*-amino benzenesulfonic acid were added into a flask of 100 mL, respectively. Afterward, 0.2 g of $NaNO_2$ was added into the flask, and after the $NaNO_2$ was completely dissolved, 10 mL of ice water and 1 mL of HCl (36%) were added. The above solution was then stirred under about 0 °C for 15 min, and diazonium salt was obtained.

During the third step, the solution of *p*-amino benzenesulfonic acid diazonium salt was added into the solution of the prereduced GO drop by drop, and then, the mixed solution was kept in an ice bath and stirred for 2−4 h. Afterward, the mixed solution was centrifuged, and the precipitate was collected and cleaned. Preliminary SGO was obtained.

During the fourth step, preliminary SGO was re-reduced to remove the redundant oxygen-containing groups, such as hydroxyl and carboxyl. First, a certain amount of hydrazine hydrate was added into the preliminary SGO solution, which was then stirred under 100 °C for 24 h. Second, several drops of Na_2CO_3 solution (5%) was added to precipitate and remove the slightly sulfonated GO. Third, the supernate was centrifuged under 10,000 rpm to get SGO, which was initially washed repeatedly with deionized water and then dissolved with deionized water under ultrasound.

Methane Hydrate Formation. In this work, all the methane hydrate formation experiments were carried out in an 80 mL reactor, which was made of 316L stainless steel and with the maximum pressure capability of 20 MPa. As shown by the schematic diagram in Figure 1, the reactor was placed in a thermostatic water bath (253.15−323.15 K) and equipped one PT100 temperature transducer with the uncertainty of 0.01 K and one SDD-601 pressure transducer with the uncertainty of 0.01 MPa. Moreover, a magnetic stirring apparatus (0−1000 rpm) was installed under the reactor, and a rotor with the size of 6 mm × 15 mm (diameter × length) was used for stirring.

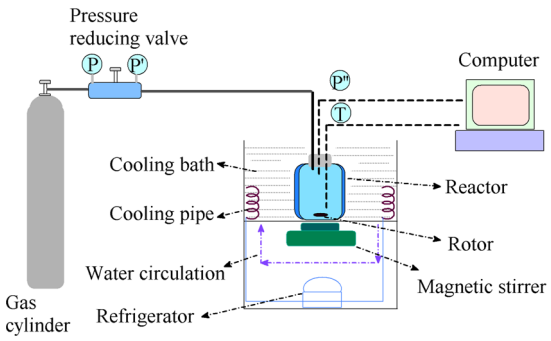

Figure 1. Schematic diagram of the methane hydrate formation apparatus.

During the methane hydrate formation experiments, the reactor was first washed with deionized water three times and then charged with 10 mL of reaction solution (fresh solution was used for each experiment); afterward, the cooling system and stirring of 300 rpm were turned on. After the reaction temperature (275.15 K) was reached, the reactor was purified with methane three times and then pressurized with methane to 6 MPa. The evolutions of temperature and pressure during the methane hydrate formation process were recorded by a computer.

DOI: 10.1021/acssuschemeng.7b00846
ACS Sustainable Chem. Eng. 2017, 5, 6597−6604

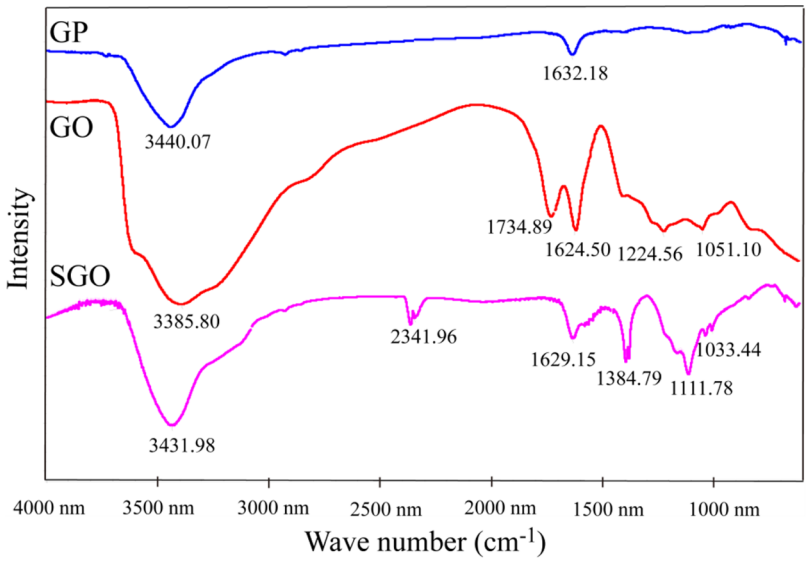

Figure 2. Infrared spectroscopy of graphene (GP), graphene oxide (GO), and sulfonated graphene oxide (SGO).

The methane consumption at time t (n_t) during the hydrate formation process is calculated according to eqs 1 and 2, which were derived in our previous study[23]

$$n_t = \left(\frac{P_0V_0}{z_0RT_0} - \frac{P_tV_0}{z_tRT_t}\right)\Big/\left(1 - \frac{P_t\Delta Vm}{z_tRT_t}\right) \quad (1)$$

$$z_t = 1 + \left[0.083 - 0.422 \times \left(\frac{T_c}{T_t}\right)^{1.6}\right](P_tT_c/P_cT_t) + \omega\left[0.139 - 0.172 \times \left(\frac{T_c}{T_t}\right)^{4.2}\right](P_tT_c/P_cT_t) \quad (2)$$

where P represents the pressures in the reactor; V represents the volumes of the gas phase in the reactor; T represents the temperatures in the reactor; R represents the universal gas constant; m represents the hydration number;[24] ΔV represents the molar volume difference between methane hydrates and water;[25] z represents the compressibility factors. For methane, T_c, P_c, and ω are 190.6 K, 4.599 MPa, and 0.012, respectively.[26] Subscripts 0 and t represent the time during the hydrate formation process.

Then the hydrate storage capacity (c_s) at time t is calculated by

$$c_s = n_t[V_{mg}V_{mw}/V_w(V_{mw} + \Delta V)] \quad (3)$$

where V_{mg} and V_{mw} represent the molar volumes of gas and water, respectively; V_w represents the volume of the initial reaction solution.

RESULTS AND DISCUSSION

Characterization of GO, GP, and SGO. Figure 2 shows the infrared spectroscopy of GO, GP, and SGO. For GO, the peak at 3440 cm^{-1} represents the stretching vibration of −OH. The peak at 1734 cm^{-1} represents the stretching vibration of carboxyl groups ($-COO^-$) on the edges of the layer planes or conjugated carbonyl groups (C═O). The peak at 1051 cm^{-1} represents the vibration of C−O. The peak at 1224 cm^{-1} represents the vibration of C−O−C.[27] All four peaks above indicated that GO was successfully obtained through the oxidation of graphite. After reduction by hydrazine hydrate (for GP), most of the characteristic peaks disappeared, which confirmed the successful reduction of GO and the formation of GP. For SGO, the peaks at 3440, 1734, 1224, and 1051 cm^{-1} were weakened or disappeared compared with GO, which was caused by reduction during the sulfonation of GO and indicated the obvious reduction of GO. At the same time, the stretching vibration peaks of S═O (1111 and 1033 cm^{-1}) appeared, and this denoted that the $-SO_3^-$ groups were successfully grafted on the GO nanosheets.

Figure 3 shows the XRD spectra of graphite, GP, GO, and SGO. For graphite, there was a strong diffraction peak at 2θ of

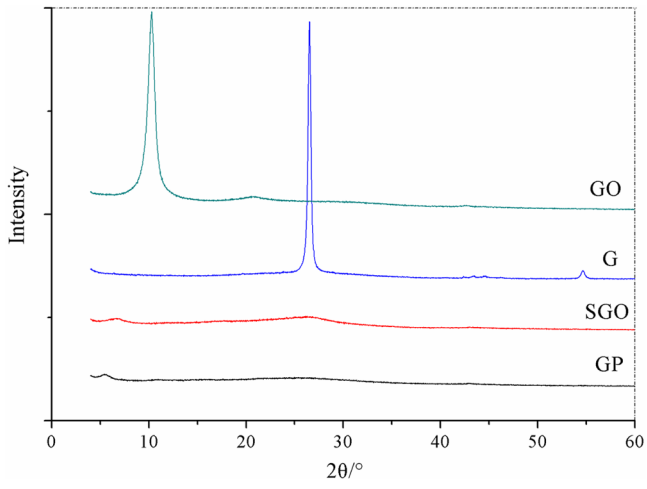

Figure 3. XRD spectra of graphite (G), graphene (GP), graphene oxide (GO), and sulfonated graphene oxide (SGO).

26.56°, while for GO a strong diffraction peak at 2θ of 11.60° was observed. The peak at 26.56° completely disappeared, indicating the successful insertion of oxygen-containing groups between graphitic layers and the successful oxidation of graphite.[28] For GP and SGO, no obvious diffraction peak was observed, and this was because after reduction or sulfonation, GP or SGO was only a few layers.[29]

Figure 4 shows the TEM photos of graphite, GP, GO, and SGO. For graphite, an obvious multilayer structure was observed, while after oxidation and ultrasonic dispersion (for GO), a single- or double-layered structure was obtained. The graphene obtained through the reduction of graphene oxide with a hydrazine hydrate also showed as a thin-layered

DOI: 10.1021/acssuschemeng.7b00846
ACS Sustainable Chem. Eng. 2017, 5, 6597−6604

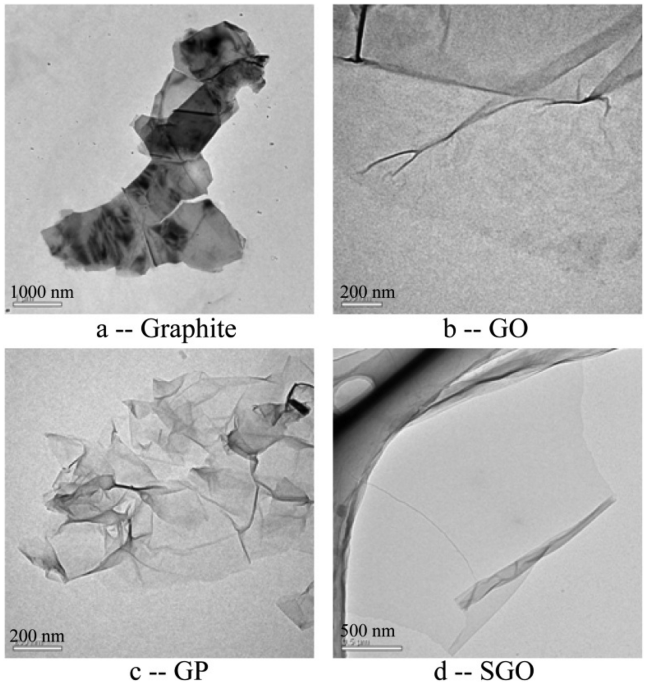

Figure 4. TEM photos of graphite, GP, GO, and SGO.

structure. After sulfonation, a single-layered structure was still retained well, and this indicated that the sulfonation might merely take place at the surface or the edge of the nanosheets.

In summary, we confirmed the successful preparation of GP, GO, and SGO, and the possible schematic diagram of the structures of GP, GO, and SGO are shown in Figure 5. For GP, a thin layer of nanosheets was obtained. For GO, carboxyl groups were grafted on the edge of the nanosheet, and hydroxyl and epoxy groups were grafted on the nanosheet. For SGO, the oxygen-containing groups were mostly reduced, and sulfonic acid groups were successfully grafted on the nanosheets.

Methane Hydrate Formation. In this work, we first used the turbid liquid of GP for methane hydrate formation, which was prepared by dispersing GP powder into deionized water and ultrasonically dispersing before usage. Moreover, deionized water was also used for comparison. The evolutions of methane consumption during hydrate formation with the turbid liquid of GP and deionized water are shown in Figure 6, and the values of hydrate formation period, hydrate formation rate, and methane storage capacity are shown in Table S1. When deionized water was used, the main hydrate formation period lasted about 1100 min, with the hydrate formation rate of 0.0041 mmol gas min^{-1} mL^{-1} water and methane storage capacity of 86.8 v/v. When GP was used, obvious promotion to methane hydrate formation was observed compared with deionized water. For GP of 0.25, 0.5, and 0.75 g/L, the main hydrate formation periods were shortened to 426.3 ± 167.2, 516 ± 106.6, and 375.7 ± 174.6 min, respectively. The hydrate formation rates were improved to 0.021 ± 0.008, 0.016 ± 0.004, and 0.023 ± 0.008 mmol gas min^{-1} mL^{-1} water, respectively; the storage capacities were increased to 139.8 ± 1.7, 142.7 ± 5.0, and 132.0 ± 5.8 v/v, respectively. In other words, compared with deionized water, GP could reduce the hydrate formation period and improve the hydrate formation rate and storage capacity by about 45−80%, 190−660%, and 45−70%, respectively.

In the methane hydrate formation with deionized water, hydrates formed initially at the gas/liquid interface and then grew downward into the liquid phase. However, the hydrates formed at the interface retarded the diffusion of gas molecules into the liquid phase and therefore led to slow hydrate formation.[30] As a result, even under the magnetic stirring of 300 rpm, hydrates grew slowly in the deionized water system. When GP was used to promote methane hydrate formation, a large number of nanosheets of GP were dispersed evenly in the liquid phase. On one hand, the nanosheets could produce numerous nanometric heterogeneous nuclei, which could provide a large number of active sites for hydrate nucleation. On the other hand, the nanosheets of GP produced high heat

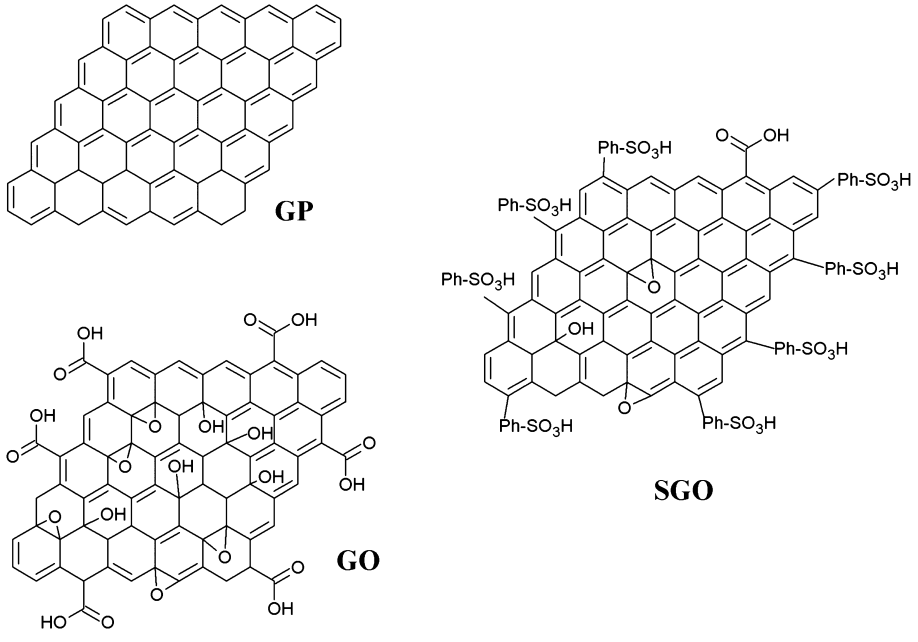

Figure 5. Schematic diagram of structures of GP, GO, and SGO.

DOI: 10.1021/acssuschemeng.7b00846
ACS Sustainable Chem. Eng. 2017, 5, 6597−6604

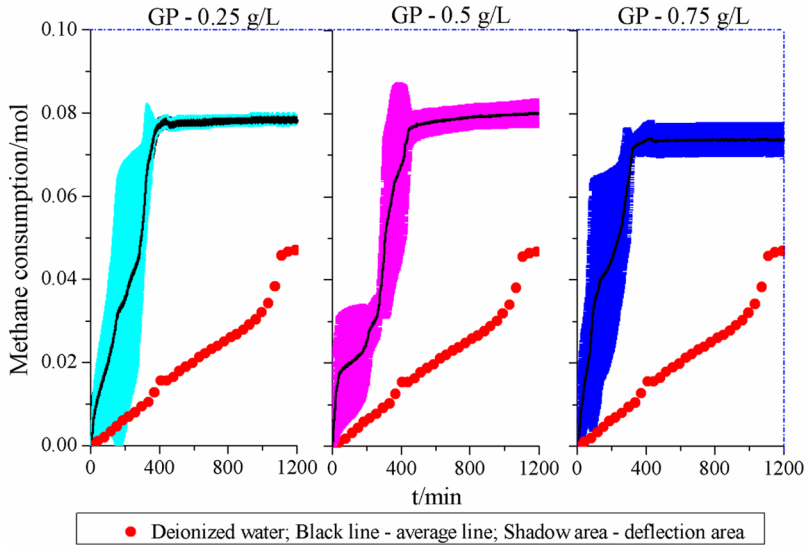

Figure 6. Evolution of methane consumption during methane hydrate formation with GP of different concentrations and deionized water (initial conditions: 6 MPa, 275.15 K, 300 rpm).

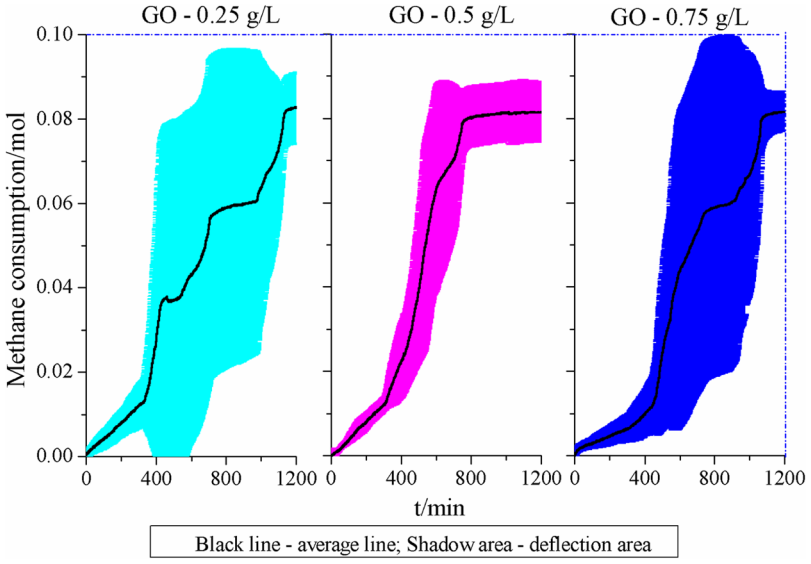

Figure 7. Evolution of methane consumption during methane hydrate formation with GO of different concentrations (initial conditions: 6 MPa, 275.15 K, 300 rpm).

transfer efficiency, which could remove the heat generated during hydrate formation rapidly and therefore resulted in efficient promotion to hydrate formation.[19]

Afterward, we used GO to promote methane hydrate formation, and the results are shown in Figure 7 and Table S1. For GO of 0.25, 0.5, 0.75 g/L, the main hydrate formation periods were 859.3 ± 385.1, 912.7 ± 133.4, and 723.3 ± 101.9 min, respectively, much longer than those of GP at the same concentration. The hydrate formation rates were 0.012 ± 0.005, 0.009 ± 0.002, and 0.011 ± 0.002 mmol gas min^{-1} mL^{-1} water, respectively, much lower than those of GP at the same concentration. The storage capacities were 148.1 ± 13.9, 143.9 ± 8.0, and 144.5 ± 10.2 v/v, respectively, slightly higher than those of GP at the same concentration. This indicated that GO produced poorer promotion compared with GP, especially for the hydrate formation rate (as shown in Figure 8), which might be caused by the different structures of GP and GO. Compared with GP, as shown in Figure 5, many oxygen-containing groups (e.g., hydroxyl, carboxyl, and epoxy group) existed on the nanosheets of GO. On one hand, the oxygen-containing groups produced strong interaction with water molecules and therefore reduce the water activity.[21] On the other hand, the existence of oxygen-containing groups destroyed the conjugated structure of the nanosheets and hence decreased the heat transfer efficiency. As a result, GO resulted in a much lower hydrate formation rate compared with GP.

Given that SDS has been confirmed as the most efficient kinetic promoter for gas hydrate formation, we grafted $-SO_3^-$ groups to the nanosheets of GO via sulfonation to prepared $-SO_3^-$-coated nanosheets of SGO. Moreover, SGO was also reduced with hydrazine hydrate to reduce the impact of the oxygen-containing groups on the structure and property of SGO. Figure 9 shows the evolution of methane consumption with SGO of different concentrations, and the values of hydrate formation period, hydrate formation rate, and methane storage capacity are shown in Table S1. For SGO of 0.25, 0.5, 0.75 g/L,

DOI: 10.1021/acssuschemeng.7b00846
ACS Sustainable Chem. Eng. 2017, 5, 6597−6604

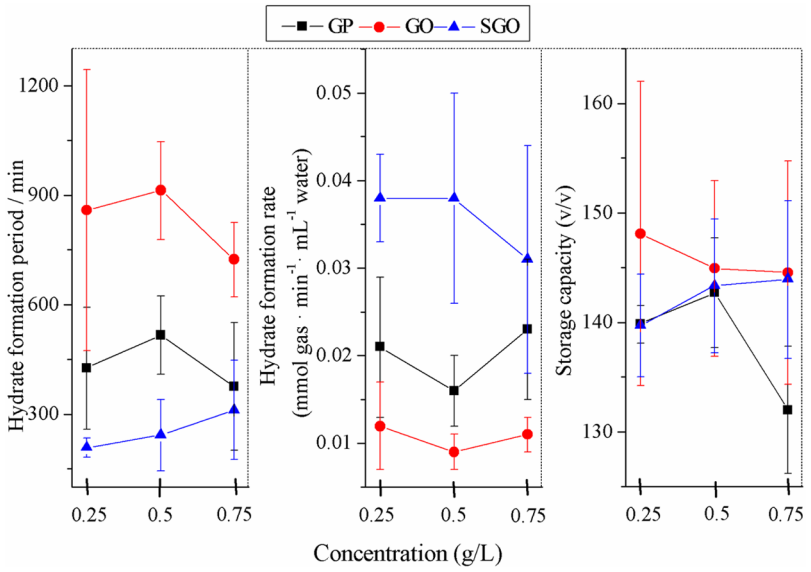

Figure 8. Comparison of hydrate formation period and rate and storage capacity of methane hydrate formation with different kinetic promoters (initial conditions: 6 MPa, 275.15 K, 300 rpm).

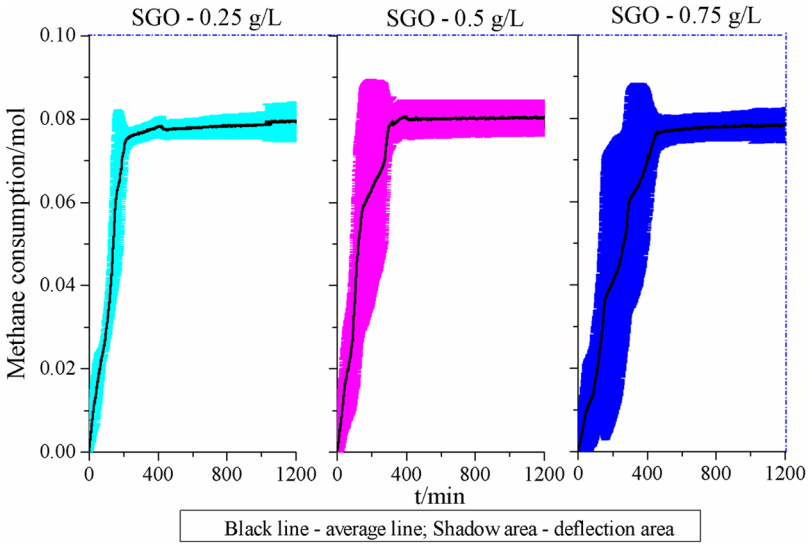

Figure 9. Evolution of methane consumption during methane hydrate formation with SGO of different concentrations (initial conditions: 6 MPa, 275.15 K, 300 rpm).

the main hydrate formation periods were 208.7 ± 26.6, 242.3 ± 97.6, and 312 ± 135.5 min, respectively, obviously shorter than those of GP and GO at the same concentration. The hydrate formation rates were 0.038 ± 0.005, 0.038 ± 0.012, and 0.031 ± 0.013 mmol gas min^{-1} mL^{-1} water, respectively, much higher than those of GP and GO at the same concentration. The storage capacities were 139.7 ± 4.7, 143.3 ± 6.1, and 143.9 ± 7.2 v/v, respectively, similar to those of GP and GO at the same concentration. This indicated that SGO produced the most efficient promotion to methane hydrate formation among GP, GP, and SGO, especially for the hydrate formation rate, as shown in Figure 8. On one hand, as most of the oxygen-containing groups had been reduced during preparation, the inhibition to water activity was removed. On the other hand, as reported in our previous study,[31] when we used the $-SO_3^-$-coated nanospheres to promote methane hydrate formation, significant efficient promotion was achieved because the nanospheres could provide a large interface where methane molecules could be adsorbed and water molecules could be associated. Similarly, when the $-SO_3^-$-coated nanosheets of SGO were used, both methane and water molecules could be adsorbed on the surface of the nanosheets and therefore led to rapid hydrate formation.

Figure 10 shows the evolutions of methane consumption during methane hydrate formation with SGO and SDS. When SDS of 0.288 g/L was used, obvious stochasticity of hydrate formation was observed, and even no hydrate formation was observed within 1200 min during one experiment with SDS, while SGO resulted in very good repeatability of the three round of experiments. Moreover, although SDS led to rapid hydrate growth, SGO resulted in a similar hydrate formation period compared with SDS given the induction period when SDS was used. However, SGO resulted in higher final methane consumption compared with SDS, indicating higher methane storage capacity. Furthermore, with SDS as the kinetic promoter, lots of foam was generated during hydrate

DOI: 10.1021/acssuschemeng.7b00846
ACS Sustainable Chem. Eng. 2017, 5, 6597−6604

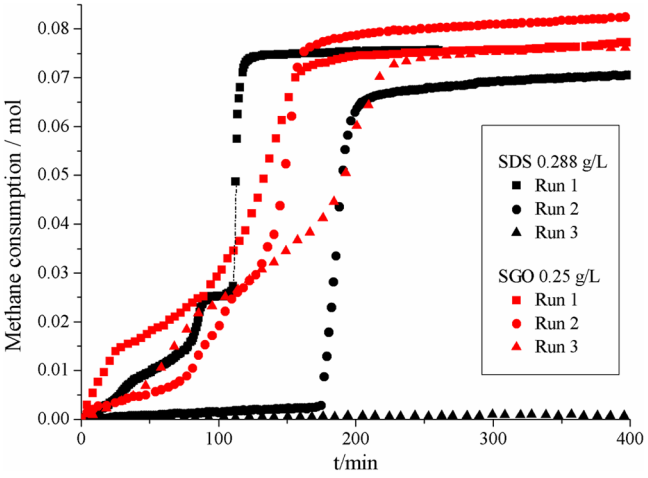

Figure 10. Comparison between the evolutions of methane consumption during methane hydrate formation with SGO and SDS of similar concentration (initial conditions: 6 MPa, 275.15 K, 300 rpm).

dissociation, as shown in Video S1, which seriously impacted the application of gas hydrates and caused the loss of the kinetic promoter. while when SGO was used, as shown in Video S2, no foam was observed during hydrate dissociation. Therefore, we proposed that SGO might produce good recycling performance in hydrate formation−dissociation and was more suitable for promoting hydrate-based natural gas storage and transportation, which will be researched in our following work. In general, the $-SO_3^-$-coated nanosheets of SGO developed in this work could produce better promotion to methane hydrate formation compared with SDS and avoid the defects of SDS in gas hydrates dissociation, which is of great potential in hydrate-based natural gas storage and transportation.

CONCLUSION

Here, $-SO_3^-$-coated nanosheets of GO (SGO) were prepared by grafting $-SO_3^-$ groups on nanosheets of GO, which were then applied to promote methane hydrate formation, and GP and GO were also used for comparison. With GP of 0.25, 0.5, 0.75 g/L as kinetic promoters, methane hydrate formation could be finished within 426.3 ± 167.2, 516 ± 106.6, and 375.7 ± 174.6 min, respectively, much shorter than those with GO, which were 859.3 ± 385.1, 912.7 ± 133.4, and 723.3 ± 101.9 min, respectively. However, when SGO of the same concentrations were applied, hydrate formation could be completed within 208.7 ± 26.6, 242.3 ± 97.6, and 312 ± 135.5 min, respectively, with storage capacity reaching 139.7 ± 4.7, 143.3 ± 6.1, and 143.9 ± 7.2 v/v, respectively, similar as those of GP and GO, indicating much better promotion compared with GP and GO. Furthermore, SGO even produced better promotion to methane hydrate formation compared with SDS and avoided foam generation during hydrate dissociation, which has great potential in hydrate-based natural gas storage and transportation.

ASSOCIATED CONTENT

Supporting Information

The Supporting Information is available free of charge on the ACS Publications website at DOI: 10.1021/acssuschemeng.7b00846.

Detailed data of hydrate formation period, formation rate and storage capacity of methane hydrate formation with different promoters. (PDF)

Video S1 of dissociation morphology of methane hydrates formed with SDS of 0.288 g/L. (AVI)

Video S2 of dissociation morphology of methane hydrates formed with SGO of 0.25 g/L. (AVI)

AUTHOR INFORMATION

Corresponding Authors

*Fei Wang. E-mail: wang_fei@qibebt.ac.cn. Tel:+86-532-58782861.

*Sheng-Jun Luo. E-mail: luosj@qibebt.ac.cn. Tel: +86-532-80662750.

*Rong-Bo Guo. E-mail: guorb@qibebt.ac.cn. Tel: +86-532-80662708.

ORCID

Fei Wang: 0000-0002-2811-7636

Rong-Bo Guo: 0000-0003-1880-2960

Author Contributions

‖Fei Wang and Han-Lin Meng contributed equally.

Notes

The authors declare no competing financial interest.

ACKNOWLEDGMENTS

This work was supported by the China Postdoctoral Science Foundation funded project (2017M612370), National Science and Technology Support Program (2015BAL04B02).

REFERENCES

(1) Sloan, E. D.; Koh, C. A. In *Clathrate Hydrates of Natural*; Gases; Heinemann, H., Speight, J. G., Eds.; CRC Press: Boca Raton, 2007; Chapter 2, pp 60−63.

(2) Gudmundsen, J.; Borrehaug, A. Frozen Hydrate for Transport of Natural Gas. Second International Symposium on Gas Hydrates; Toulouse, 1996; pp 415−422.

(3) Yevi, G. Y.; Rogers, R. E. Storage of fuel in hydrates for natural gas vehicles (NGVs). *J. Energy Resour. Technol.* **1996**, *118*, 209−213.

(4) Zhong, Y.; Rogers, R. E. Surfactant effects on gas hydrate formation. *Chem. Eng. Sci.* **2000**, *55*, 4175−4187.

(5) Lin, W.; Chen, G. J.; Sun, C. Y.; Guo, X. Q.; Wu, Z. K.; Liang, M. Y.; Chen, L. T.; Yang, L. Y. Effect of surfactant on the formation and dissociation kinetic behavior of methane hydrate. *Chem. Eng. Sci.* **2004**, *59*, 4449−4455.

(6) Ganji, H.; Manteghian, M.; Omidkhah, M. R.; Rahimi Mofrad, H.; Sadaghiani zadeh, K. Effect of Different Surfactants on Methane Hydrate Formation Rate, Stability and Storage Capacity. *Fuel* **2007**, *86*, 434−441.

(7) Wang, F.; Jia, Z. Z.; Luo, S. J.; Fu, S. F.; Wang, L.; Shi, X. S.; Wang, C. S.; Guo, R. B. Effects of Different Anionic Surfactants on Methane Hydrate Formation. *Chem. Eng. Sci.* **2015**, *137*, 896−903.

(8) Okutani, K.; Kuwabara, Y.; Mori, Y. H. Surfactant Effects on Hydrate Formation in an Unstirred Gas/liquid System: An Experimental Study Using Methane and Sodium Alkyl Sulfates. *Chem. Eng. Sci.* **2008**, *63*, 183−194.

(9) Watanabe, K.; Imai, S.; Mori, Y. H. Surfactant Effects on Hydrate Formation in an Unstirred Gas/liquid System: An Experimental Study Using HFC-32 and Sodium Dodecyl Sulfate. *Chem. Eng. Sci.* **2005**, *60*, 4846−4857.

(10) Zhang, C. S.; Fan, S. S.; Liang, D. Q.; Guo, K. H. Effect of Additives on Formation of Natural Gas Hydrate. *Fuel* **2004**, *83*, 2115−2121.

(11) Daimaru, T.; Yamasaki, A.; Yanagisawa, Y. Effect of Surfactant Carbon Chain Length on Hydrate Formation Kinetics. *J. Pet. Sci. Eng.* **2007**, *56*, 89−96.

(12) Yoslim, J.; Linga, P.; Englezos, P. Enhanced Growth of Methane−propane Clathrate Hydrate Crystals with Sodium Dodecyl Sulfate, Sodium Tetradecyl Sulfate, and Sodium Hexadecyl Sulfate Surfactants. *J. Cryst. Growth* **2010**, *313*, 68−80.
(13) Kwon, Y. A.; Park, J. M.; Jeong, K. E.; Kim, C. U.; Kim, T. W.; Chae, H. J.; Jeong, S. Y.; Yim, J. H.; Park, Y. K.; Lee, J. D. Synthesis of Anionic Multichain Type Surfactant and Its Effect on Methane Gas Hydrate Formation. *J. Ind. Eng. Chem.* **2011**, *17*, 120−124.
(14) Kumar, A.; Bhattacharjee, G.; Kulkarni, B. D.; Kumar, R. Role of Surfactants in Promoting Gas Hydrate Formation. *Ind. Eng. Chem. Res.* **2015**, *54*, 12217−12232.
(15) Wang, F.; Liu, G. Q.; Meng, H. L.; Guo, G.; Luo, S. J.; Guo, R. B. Improved Methane Hydrate Formation and Dissociation with Nanosphere-Based Fixed Surfactants As Promoters. *ACS Sustainable Chem. Eng.* **2016**, *4*, 2107−2113.
(16) Veluswamy, H. P.; Hong, Q. W.; Linga, P. Morphology Study of Methane Hydrate Formation and Dissociation in the Presence of Amino Acid. *Cryst. Growth Des.* **2016**, *16*, 5932−5945.
(17) Stankovich, S.; Dikin, D. A.; Dommett, G. H. B.; Kohlhaas, K. M.; Zimney, E. J.; Stach, E. A.; Piner, R. D.; Nguyen, S. T.; Ruoff, R. S. Graphene-based composite materials. *Nature* **2006**, *442*, 282−286.
(18) Ghozatloo, A.; Hosseini, M.; Shariaty-Niassar, M. Improvement and enhancement of natural gas hydrate formation process by Hummers' graphene. *J. Nat. Gas Sci. Eng.* **2015**, *27*, 1229−1233.
(19) Hosseini, M.; Ghozatloo, A.; Shariaty-Niassar, M. Effect of CVD graphene on hydrate formation of natural gas. *J. Nanostruct. Chem.* **2015**, *5*, 219−226.
(20) Rezaei, E.; Manteghian, M.; Tamaddondar, M. Kinetic Study of Ethylene Hydrate Formation in Presence of Graphene Oxide and Sodium Dodecyl Sulfate. *J. Pet. Sci. Eng.* **2016**, *147*, 857−863.
(21) Kim, D.; Kim, D. W.; Lim, H. K.; Jeon, J.; Kim, H.; Jung, H. T.; Lee, H. Inhibited phase behavior of gas hydrates in graphene oxide: influences of surface and geometric constraints. *Phys. Chem. Chem. Phys.* **2014**, *16*, 22717−22722.
(22) Wu, J. L.; Shen, X. P.; Jiang, L.; Wang, K.; Chen, K. M. Solvothermal synthesis and characterization of sandwich-like graphene/ZnO nano-composites. *Appl. Surf. Sci.* **2010**, *256*, 2826−2830.
(23) Wang, F.; Luo, S. J.; Fu, S. F.; Jia, Z. Z.; Dai, M.; Wang, C. S.; Guo, R. B. Methane Hydrate Formation with Surfactants Fixed on the Surface of Polystyrene Nano-spheres. *J. Mater. Chem. A* **2015**, *3*, 8316−8323.
(24) Gutt, C.; Asmussen, B.; Press, W.; Johnson, M. R.; Handa, Y. P.; Tse, J. S. The Structure of Deuterated Methane-hydrate. *J. Chem. Phys.* **2000**, *113*, 4713.
(25) Makogon, Y. F. In *Hydrates of Hydrocarbons*; PennWell Books: Tulsa, OK, 1997; pp 35−37.
(26) Smith, J. M.; Van, N. H. C.; Abbott, M. M. In *Introduction to Chemical Engineering Thermodynamics*, 6th ed.; McGraw-Hill Education: Singapore, 2001; pp 96−98.
(27) Titelman, G. I.; Gelman, V.; Bron, S.; Khalfin, R. L.; Cohen, Y.; Bianco-Peled, H. Characteristics and microstructure of aqueous colloidal dispersions of graphite oxide. *Carbon* **2005**, *43*, 641−649.
(28) Long, D.; Li, W.; Ling, L.; Miyawaki, J.; Mochida, I.; Yoon, S. H. Preparation of Nitrogen-Doped Graphene Sheets by a Combined Chemical and Hydrothermal Reduction of Graphene Oxide. *Langmuir* **2010**, *26*, 16096−16102.
(29) Liu, F.; Sun, J.; Zhu, L.; Meng, X.; Qi, C.; Xiao, F. S. Sulfated graphene as an efficient solid catalyst for acid-catalyzed liquid reactions. *J. Mater. Chem.* **2012**, *22*, 5495−502.
(30) Lee, J. D.; Song, M.; Susilo, R.; Englezos, P. Dynamics of Methane−Propane Clathrate Hydrate Crystal Growth from Liquid Water with or without the Presence of *n*-Heptane. *Cryst. Growth Des.* **2006**, *6*, 1428−1439.
(31) Wang, F.; Guo, G.; Luo, S. J.; Guo, R. B. Preparation of -SO_3^--coated nanopromoters for methane hydrate formation: effects of the existence pattern of -SO_3^- groups on the promotion efficiency. *J. Mater. Chem. A* **2017**, *5*, 2640−2648.

DOI: 10.1021/acssuschemeng.7b00846
ACS Sustainable Chem. Eng. 2017, 5, 6597−6604